Relative Humidity Sensor Based on Double Sagnac Interferometers and Vernier Effect

Xuefang Zhou, Yanxu Duan, Xiaotong Xu, and Yuansheng Xu

***Abstract*—A double Sagnac interferometer (DSI) and vernier effect sensor for relative humidity (RH) is proposed and experimentally implemented, in which two single Sagnac interferometers (SI1 and SI2) cascaded in parallel to construct the structure of the sensor. Owing to the approximate free spectral range (FSR) of the SI1 and SI2, the proposed sensor can produce fundamental and harmonic vernier effect. Theoretical analysis shows that the RH sensitivity of the sensor is only related to the lengths of polarization-maintaining fibers (PMFs). The experimental results show that in the range of 30∼80%RH, the RH sensitivities of the spectral envelope can reach −0.48 nm/%RH, which is 60 times higher than that measured by the single Sagnac interferometer sensor (8 pm/%RH). The experimental results are consistent with the theoretical analysis. The proposed sensor has the superiorities of high sensitivity, good repeatability, simple fabrication, and compact size, and it has potential applications in the areas of biopharmaceuticals, environmental monitoring, food processing, and microbial sensing.**

***Index Terms*—Double sagnac interferometer, fiber sensor, relative humidity, vernier effect.**

I. Introduction

RELATIVE humidity (RH) refers to the ratio of the actual water content of the air to the theoretical maximum water content, whose measurement or monitoring is particularly important in human daily life and industrial production, such as the spread of COVID-19, preservation time of agricultural and sideline products, the service life of the precision instrument and so on [1], [2], [3], [4]. With the development of science and technology, RH sensors emerges, and developed rapidly during the past twenty years, while the conventional RH sensors are mainly based on electric conduction technology, which have the disadvantages such as bulky size and difficult signal process, and then makes it less possible to be coupled to automatic controlling system. The appearance of optical fiber sensors can make up for this defect because optical fiber sensors have some advantages of high-temperature resistance, larger dynamic range, strong adaptability, anti-electromagnetic interference [5], and so on. Therefore, various fiber RH sensors with different structures have been developed and reported successively. Among them, interferometric fiber optic sensors are the fastest developing sensors in recent three years. There are four common interferometric sensors, including Mach-Zehnder interferometers (MZIs) [6], [7], [8], Fabry-Perot interferometers (FPIs) [9], [10], [11], Sagnac interferometers (SI) [12], [13], [14], Michelson interferometers (MI) [15], [16]. In the 2022 year, Xin Ding and his groups [8] proposed a balloon-like structure fiber interferometer with GO nanomaterial coating for humidity detection, whose sensitivity is 0.449 nm/%RH in the measurement range of less than 50%RH, the sensitivity isn't very high, and the sensor structure is difficult to manufacture. In the 2022 year, Hailin Chen and his companions [10] proposed a parallel optical fiber FPI and vernier effect sensor for simultaneous high sensitivity measurement of RH and temperature, the sensitivity of RH and temperature is up to −11.388 nm/%RH and 18.436 nm/°C, respectively. In the 2021 year, Yuanfang Zhao and his groups [12] proposed a sucrose concentration sensor by utilizing a fiber Sagnac interferometer with no-core fiber (SI-NCF) based on the vernier effect. In these vernier effect-based sensors, the spectrum of the sensors forms a large envelope, and the sensitivity of the sensor can be amplified by tracking the movement of the envelope.

In our previous research, we demonstrated fiber sensor configurations of cascaded hybrid types fiber interferometers [17], [18], [19]. The vernier effect of the hybrid interferometer has been significantly improved in temperature measurement. Therefore, it is used to fabricate temperature sensors based on cascaded interferometers, and high-temperature sensitivity is obtained. In these previous works, the hybrid-types fiber interferometer consisting of two different interferometers was used for temperature sensing or RH demonstrations. In this paper, a DSI for RH measurement based on the vernier effect is first proposed and demonstrated. The sensitivity of the RH sensor is improved by the vernier effect which generates between the two Sagnac interferometers with different lengths of PMF. The proposed sensor has the advantages of stable performance, simple production, and high repeatability.

II. Sensor Fabrication and Principle

In optical fiber sensing, the cascade of two interferometers can produce periodic vernier interference fringes, and the interference fringes will be changed sharply with the physical

Manuscript received 24 February 2023; revised 16 March 2023; accepted 17 March 2023. Date of publication 21 March 2023; date of current version 30 March 2023. This work was supported in part by the Zhejiang Province Science and Technology Plan Projects under Grant LGG19F050001 and in part by the Key Laboratory of Data Storage and Transmission Technology of Zhejiang Province. *(Corresponding authors: Xuefang Zhou; Yuansheng Xu.)*

Xuefang Zhou, Yanxu Duan, and Xiaotong Xu are with the School of Communication and Engineering, Hangzhou Dianzi University, Hangzhou 310018, China (e-mail: zhouxf@hdu.edu.cn; 15280066@qq.com; 2236938724@qq.com).

Yuansheng Xu is with the Department of Emergency, Affiliated Hangzhou First People's Hospital, Zhejiang University School of Medicine, Hangzhou 310006, China (e-mail: xys0912@163.com).

Digital Object Identifier 10.1109/JPHOT.2023.3259952

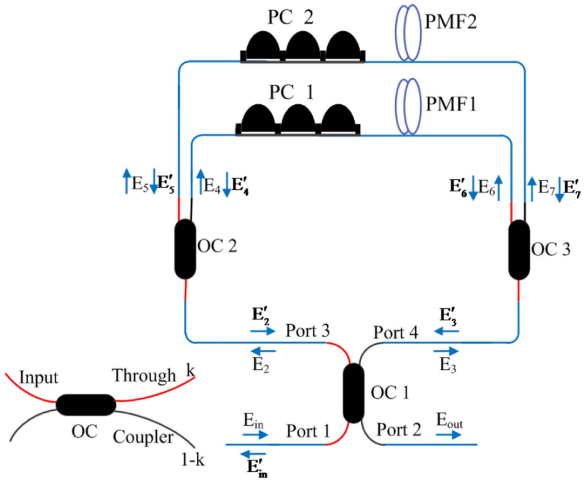

Fig. 1. The schematic diagram of the proposed sensor.

parameters (cavity length, refractive index, fringe fineness) of the cascaded interferometer. In addition, the interference fringes are periodically changed, and the sensors can be realized by demodulating the envelope of the interference fringes. The schematic diagram of the proposed RH sensor based on the vernier effect with a DSI cascaded in parallel is shown in Fig. 1, which is composed of two sections of PMF, two polarization controllers (PCs), two three-ports OCs, and a four-ports OC.

According to the coupled-mode theory, its transmission characteristic matrix can be expressed as

$$\boldsymbol{T}_{\mathbf{OC}} = \begin{pmatrix} \sqrt{1-k} & \mathbf{j}\sqrt{k} \\ \mathbf{j}\sqrt{k} & \sqrt{1-k} \end{pmatrix} \tag{1}$$

Where: k is the coupling ratio of OC.

When the incident light enters the PMF, there will be a certain angle between the PMF and the ordinary single-mode fiber (SMF). Let the angle between the PMF and the X axis of the fixed experimental coordinate system is θ_1, that is, the coordinate rotation matrix can be expressed as

$$\boldsymbol{R}(\theta_1) = \begin{pmatrix} \cos\theta_1 & \sin\theta_1 \\ -\sin\theta_1 & \cos\theta_1 \end{pmatrix} \tag{2}$$

The transmission matrix of PMF can be expressed as

$$\boldsymbol{T}_{\mathbf{PMF}} = \begin{pmatrix} e^{-\mathbf{j}\varphi} & 0 \\ 0 & e^{-\mathbf{j}\varphi} \end{pmatrix} \tag{3}$$

Among it, $\varphi = \pi\Delta n L_{PMF}/\lambda$, L_{PMF} is the length of the PMF, Δn is the effective refractive index difference between the fast and slow axes of the PMF. Because the phase difference introduced by the light field through the PMF clockwise and counterclockwise is the same, the transmission matrix of the reverse light through the PMF is the same.

Assume that the light field intensity of the incident light is

$$\boldsymbol{E}_{in} = \begin{pmatrix} E_x \\ E_y \end{pmatrix} = \begin{pmatrix} \boldsymbol{E}_{in}\cos\theta \\ \boldsymbol{E}_{in}\sin\theta \end{pmatrix} \tag{4}$$

In which E_x and $E_y$represent the decomposition of the input light field along the x and y axes respectively.

When light enters OC1, it can be described as

$$\begin{pmatrix} \boldsymbol{E}_1 \\ \boldsymbol{E}_2 \end{pmatrix} = \boldsymbol{T}_{\mathbf{OC1}} \begin{pmatrix} \boldsymbol{E}_{\mathbf{in}} \\ 0 \end{pmatrix} \tag{5}$$

Analyze the clockwise light field of the Sagnac loop as follows

$$\begin{pmatrix} \boldsymbol{E}_{5'} \\ \boldsymbol{E}_{6'} \end{pmatrix} = \begin{pmatrix} \boldsymbol{J}_{\mathbf{PMF1}} * \boldsymbol{R}(\theta_1) & 0 \\ 0 & \boldsymbol{J}_{\mathbf{PMF2}} * \boldsymbol{R}(\theta_2) \end{pmatrix} \boldsymbol{T}_{\mathbf{OC2}} \begin{pmatrix} \boldsymbol{E}_1 \\ 0 \end{pmatrix} \tag{6}$$

The electric field strength returning to OC1 port 4 is expressed as

$$\boldsymbol{E}_{2'} = \mathbf{j}\sqrt{k_3} * \boldsymbol{E}_{5'} + \sqrt{1-k_3} * \boldsymbol{E}_{6'} \tag{7}$$

Analyze the counterclockwise light field of the Sagnac loop as follows

$$\begin{pmatrix} \boldsymbol{E}_{3'} \\ \boldsymbol{E}_{4'} \end{pmatrix} = \begin{pmatrix} \boldsymbol{J}_{\mathbf{PMF1}} * \boldsymbol{R}(-\theta_1) & 0 \\ 0 & \boldsymbol{J}_{\mathbf{PMF2}} * \boldsymbol{R}(-\theta_2) \end{pmatrix} \boldsymbol{T}_{\mathbf{OC3}} \begin{pmatrix} \boldsymbol{E}_2 \\ 0 \end{pmatrix} \tag{8}$$

The electric field strength returning to port 3 of OC1 is expressed as

$$\boldsymbol{E}_{1'} = \mathbf{j}\sqrt{k_2} * \boldsymbol{E}_{4'} + \sqrt{1-k_2} * \boldsymbol{E}_{3'} \tag{9}$$

The last two beams of light meet at OC1, which can be expressed as

$$\begin{pmatrix} \boldsymbol{E}_{\mathbf{in}'} \\ \boldsymbol{E}_{\mathbf{out}} \end{pmatrix} = \boldsymbol{T}_{\mathbf{OC}} \begin{pmatrix} \boldsymbol{E}_{2'} \\ \boldsymbol{E}_{1'} \end{pmatrix} \tag{10}$$

When $k_1 = k_2 = k_3 = 0.5$ the transmission function of the transmission spectrum is expressed as

$$T = \frac{|\boldsymbol{E}_{\mathbf{out}}|^2}{|\boldsymbol{E}_{\mathbf{in}}|^2} = \frac{1}{4}(\sin\theta_1\cos\varphi_1 + \sin\theta_2\cos\varphi_2)^2 \tag{11}$$

According to the formula (11), it can be seen that the DSI's transmission spectrum is influenced by $\varphi_1 = \pi\Delta n_1 L_{PMF1}/\lambda$, $\varphi_2 = \pi\Delta n_2 L_{PMF2}/\lambda$, the increase of RH, Δn will change accordingly, which is finally resulting in the change of the output transmission spectrum.

The final interference spectrum is a superposition of the two individual SI, and the FSR1 and FSR2 are the FSR of SI1 and SI2, respectively, where SI1 is formed by cavity 1 and SI2 is formed by cavity 2. FSR1 and FSR2 can be expressed as:

$$FSR_1 = \frac{\lambda^2}{\Delta n L_1},\ FSR_2 = \frac{\lambda^2}{\Delta n L_2} \tag{12}$$

As shown in Fig. 1, two interferometers are in parallel, and the FSR of the envelope generated by the output waveform can be expressed as

$$FSR_{\mathbf{envelop}} = \frac{FSR_1 * FSR_2}{|FSR_1 - FSR_2|} = \frac{\lambda^2}{\Delta n|L_1 - L_2|} \tag{13}$$

By controlling the length of the PMF in the cascaded DSI, the optical path lengths of the two SI are different, resulting in the fundamental vernier effect. Gomes et al. creatively introduced an advanced concept of a harmonic vernier effect to further surpass

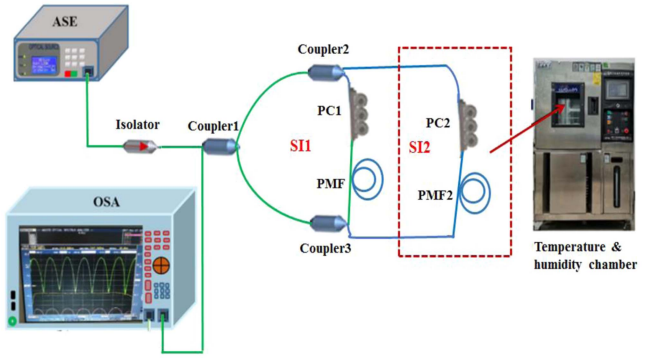

Fig. 2. Experiment setup of the proposed RH sensor system.

the limits of the traditional vernier effect [20]. Compared to the traditional vernier effect, the harmonic vernier effect allows a considerable sensitivity improvement and more flexible control of the sensitivity magnification factor. Assuming that all other conditions are the same in the DSI, the optical path degree of one SI is set to be i times that of the other, namely L2+iL1 (the value of i is the order of harmonic generation). The FSR of the envelope on the harmonic vernier effect can be expressed as

$$FSR^i_{\mathbf{harmonic}} = \left| \frac{(i+1)FSR_1 * FSR_2^i}{FSR_1 - (i+1)FSR_{\mathbf{2}}^i} \right| = (i+1)FSR^i_{\mathbf{envelope}} \quad (14)$$

It can be seen from formulas (13) and (14) that $\mathrm{FSR}_{\mathrm{envelope}}$ is affected by L1 and L2, therefore, the influence factors of $\mathrm{FSR}_{\mathrm{envelope}}$ are L1 and L2.

Compared with a single SI sensor, the envelope shift of cascaded configuration can be magnified with an impact factor M^{i},

$$M^i = \frac{FSR^i_{\mathbf{harmonic}}}{FSR_1} = \left| \frac{(i+1)FSR_2^i}{FSR_1 - (i+1)FSR_2^i} \right| = (i+1)M \quad (15)$$

The sign of the denominator $FSR_1 - (i+1)FSR_2^i$ determines the direction in which the wavelength moves. When the sign $FSR_1 - (i+1)FSR_2^i$ is positive, the slope of the sensitivity curve of FSR2 with the Vernier effect is constant. When the sign $FSR_1 - (i+1)FSR_2^i$ is negative, the sensitivity curve's slope of FSR2 with the Vernier effect will change.

III. Experiment and Discussion

The RH sensing measurement system is depicted in Fig. 2. A programmable constant temperature and humidity test chamber (QING SHENG, temi880, China) is used for relative humidity measurement. Amplified spontaneous emission (ASE) acts as a broadband light source (BBS), which emits light with a wavelength range from 1530 to 1650 nm. The light is transmitted to the sensor through the optical fiber coupler. The reflection spectrum of the sensor is collected by the OSA (Yokogawa, AQ6370D), and the resolution of the OSA is set at 0.02 nm. When SI2 conducts RH experiments separately, another parallel SI1 is removed from coupler 2 and coupler 3. The splitting ratios

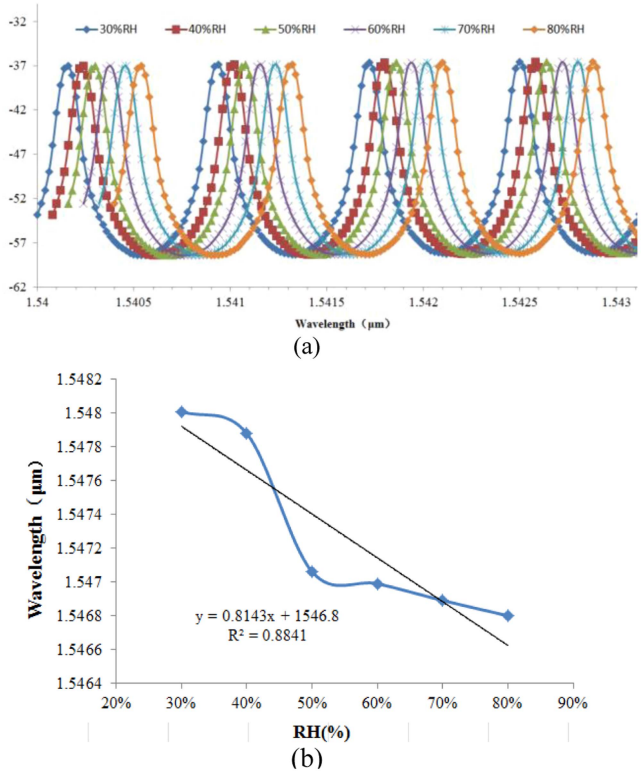

Fig. 3. (a) The experimental spectra of the single SI sensor without vernier effect under RH increasing (b) The corresponding relationships between the wavelength dip and RH of the single SI sensor.

of the coupler1, coupler2, and coupler3 are 50:50. When SI1 and SI2 are parallel for the RH experiment, because both SI1 and SI2 are sensitive to RH, to realize the vernier effect and improve RH sensitivity, the reference unit SI1 cannot be put into the test chamber.

Firstly, we put the SI2 into the test chamber to ensure sufficient contact between the sensor and RH. Under this condition, we study the SI's spectra shift response to the different RH. During the sensor calibration, we keep the temperature around 25 °C and keep the polarization state of the sensor stable and unchanged, and then change the RH value by adjusting the test chamber.

During the test, the length of PMF is 7.05 m, and the birefringence of PMF is 3.85×10^{-4}, according to the formula (12), it can be deduced that the FSR of SI2 is 0.78 nm. The measured interference spectra of the SI with different RH are depicted in Fig. 3(a). It can be noted that the resonance spectrum has a blueshift with the increasing RH value. To evaluate the RH sensitivity of the SI sensor, one typical dip at1546.8 nm is detected and the dip values at different RH are given in Fig. 3(b). When the RH increases from 30% to 80%, the wavelength shift is 0.4 nm. This result shows that the SI sensor can effectively test solutions with different RH values, and the sensitivity of the single SI sensor is 8 pm/%RH.

To improve the single SI's sensitivity, the vernier effect is introduced into the SI sensor. Fig. 4 exhibits the transmission spectrum of cascaded SI1 and SI2 in parallel with the fundamental vernier effect, where the length of PMF1 and PMF 2 is 15.05 m and 13.62 m, respectively. Due to the similarity of the

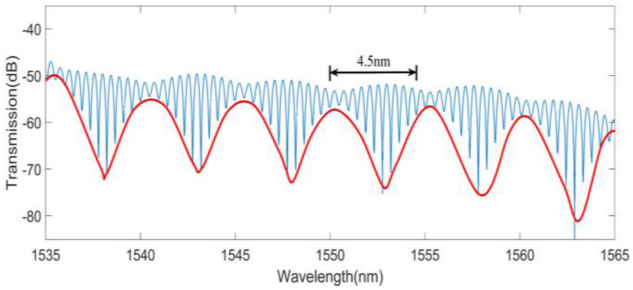

Fig. 4. Measured resonance spectra of the cascaded SI1 and SI2 in parallel.

FSR between the two interferometers, the transmission spectrum of the cascaded configuration has a superimposed envelope. The extinction ratio (ER) of the output spectrum is about 20 dB. In addition, the FSR of the DSI sensor based on the fundamental vernier effect is 4.5 nm near the wavelength of 1550 nm, which is 5.76 times of the single SI sensor, and the theoretical value of the FSR near 1550 nm is 4.16 nm according to the formula (13), there is a good agreement between theoretical calculation and experimental test. The FSR shows that this method is promising to improve the sensor's sensitivity.

As is depicted in formula (14), the reference SI1 has a length of L2 + iL1, and the sensing SI2 has a fixed length of L2, i denotes the order of the harmonic, and L1 is the detuning length. The first case in Fig. 4 corresponds to the fundamental vernier effect, where i = 0. Fig. 5(a)–(c) shows three cases corresponding to the first three harmonics, where L1 is 6.6 m and L2 = 0.2+iL1(i = 12,3) respectively. Fig. 5(a) is the simulated spectrum of the first-order harmonic vernier effect. The upper envelope FSR is 30nm and the inner envelope FSR is 60nm, which is twice as large as the upper envelope FSR. Fig. 5(b) is the simulated spectrum of the second-order harmonic vernier effect. The upper envelope FSR is 30nm and the inner envelope FSR is 90nm, which is three times that of the upper envelope FSR. Fig. 5(c) is the simulated spectrum of the third-order harmonic vernier effect. It can be seen that the more order harmonic vernier effect, then it is more difficult to observe the complete harmonic spectrum period, and then it leads to detecting the wavelength drift with difficulty. The simulation results are consistent with that of the theoretical value, and the upstream standard envelope is independent of the harmonic order. The inner envelope produced by the harmonic vernier effect is i+1 times that of the upper envelope produced by the basic vernier effect, which means that when the RH changes slightly, the spectrum produced by the harmonic vernier effect will have a larger wavelength shift, and thus resulting in a significant improvement in RH sensitivity.

Firstly, the DSI sensor's humidity sensitivity is experimentally evaluated and analyzed according to the experimental setup shown in Fig. 2, the environment temperature is controlled at 25 °C, the length of PMF1 and PMF2 are set at 15.05 m and 13.62 m, and PMF2 is put in the chamber. When the different RH is delivered to characterize the sensor performance based on the vernier effect, the transmission spectrum of the proposed sensor based on the fundamental vernier effect at different RH ranging from 30% to 80% is shown in Fig. 6(a). It can be seen

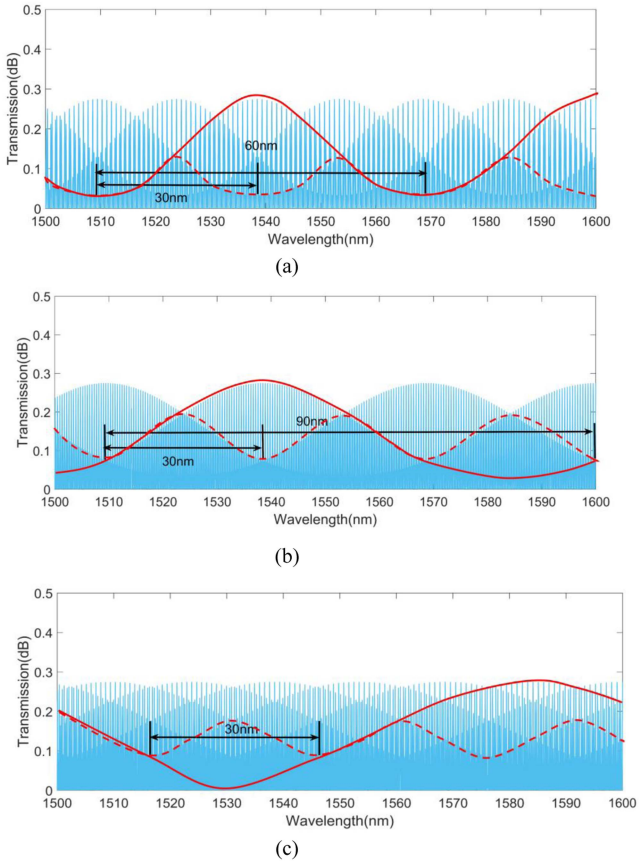

Fig. 5. Numerical simulations of the first-order harmonic vernier effect (a), and the second-order harmonic vernier effect(b), and the third-order harmonic vernier effect(c).

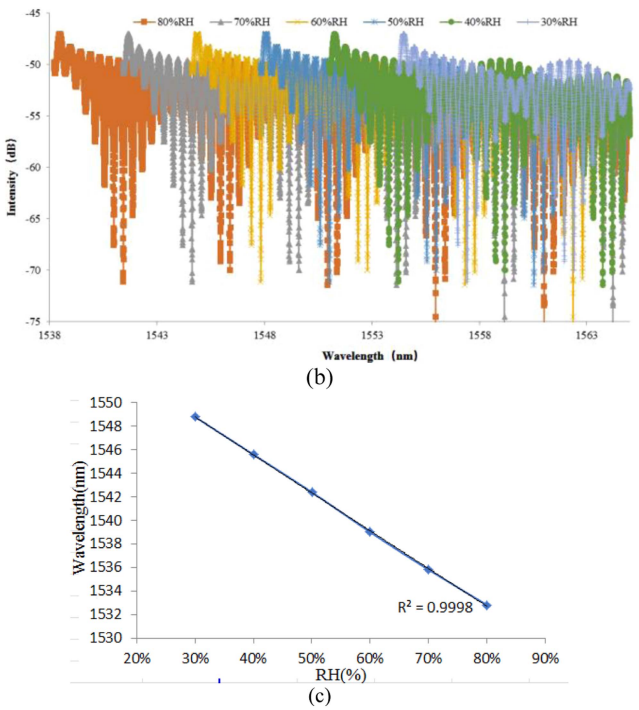

Fig. 6. (a) Transmission spectra of the DSI sensor based on vernier effect with different RH (b)the corresponding relationship between the resonance wavelength dip and the RH for the cascaded DSI with vernier effect.

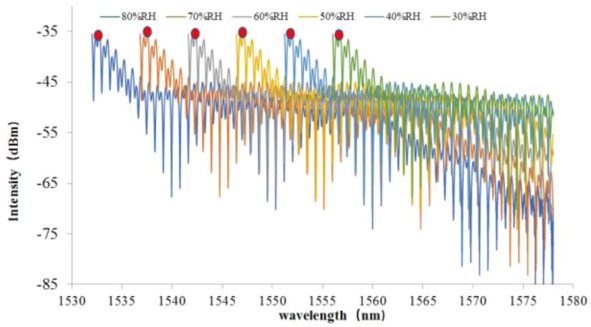

Fig. 7. Transmission spectra of the DSI sensor based on first-order harmonic vernier effect with different RH.

TABLE I
THE PERFORMANCE COMPARISON BETWEEN THE PROPOSED SENSOR WITH THE EXISTING SENSOR

Structure	Material assisted	Detection RH range	RH sensitivity (%RH)	year	Reference
MZI+FPI	GQDs-PVA	27.9%~68.5%	-0.88nm	2020	[6]
FBG+MZI	no	9.73%~80.37%	6.1pm	2019	[7]
MZI+SMF	GO	35%~90%	0.449nm	2023	[8]
FBG+FPI	no	20%~90%	22.07 pm	2018	[9]
FPI+SMF	PI+PDMS	30%~80%	-11.388nm	2022	[10]
CascadedFPI	PVA+PDMS	20%~45%	0.038nm	2022	[11]
CascadedFPI	PI	40%~85%	-344.3pm	2022	[21]
Cascaded SI	no	30%~80%	-0.48nm	2023	Our work

from Fig. 6 that when the RH increases from 30% to 80%, the envelope dips have a blue shift to 16 nm, which is since the FSR of SI2 is smaller than that of SI1 [20]. The relationship between the envelope shift and the RH is shown in Fig. 6(b), when the relative humidity is 30% $\sim$ 80%, the dip wavelength displacement is 16 nm. As we can see, the RH sensitivity is -0.32 nm/%RH, which is 40 times higher than a single SI sensor without the vernier effect. As can be seen from Fig. 6(b), the linear correlation coefficient is 0.9998, which shows good linearity.

Secondly, the output performance of the DSI sensor based on the first harmonic vernier effect wave is further studied. Fig. 7 shows the variation of dip wavelength drifts with the RH. it can be seen from Fig. 7 that when RH ranges from 30% to 80%, the dip wavelength shifts to a short wavelength direction. The envelope dips have a blue shift to 24 nm when the RH changes from 30% to 80%. As we can see, the RH sensitivity is -0.48 nm/%RH, which is 60 times higher than a single SI sensor without the vernier effect. To sum up, using the vernier effect, a cascaded DSI sensor can achieve sensitivity amplification, which is more convenient and economic.

Finally, the performance of the proposed sensor is compared and analyzed with those of the existing sensors shown in Table I. As can be seen from Table I, there are two schemes to be designed, one is to detect the RH directly by combing an optical interferometer and fiber Bragg grating (FBG), and Rui et al [7] proposed an FBG cascaded with balloon-like sensing structure with up-tapered MZI to realize the RH test, whose sensitivity is 6.1pm/%RH, and Yong et al [9] cascaded FBG and FPI to measure the RH and its sensitivity is 22.07 pm/%RH, which is relatively low. To improve the sensitivity, other schemes were designed to measure RH by using the optical interferometer structures and humidity-sensitive materials. Tong [6] et al. proposed a compact MZI and FPI structure assisted GQDs-PVA to realize the detection of RH solutions, the RH sensitivity is -0.132 nm/%RH. In summary, compared with other sensors, the proposed sensor has the comprehensive performance of simple manufacture, high sensitivity, high-cost performance, and competitiveness.

IV. CONCLUSION

In conclusion, we propose and demonstrate a cascaded DSI sensor based on the vernier effect for RH detection. We optimize the transmission spectrum of SI by adjusting the PMFs' length. The experimental results show that when the PMF1 and PMF2 lengths are 15.05 m and 13.62 m respectively, the sensitivity of the DSI sensor based on the fundamental vernier effect is -0.32 nm/%RH, which is 40 times higher than that of a single SI sensor. By tuning the length of PMF1 and PMF2 to 7.08 m and 15.08 m, e the first-order harmonic vernier effect is exactly to be generated, and the RH sensitivity of the DSI sensor is -0.48 nm/%RH. This method explores a novel RH sensor with the benefits of easy manufacture, good stability, and cost-effectiveness, it has potential applications in RH detection in biochemical engineering, food processing, and industry fields.

REFERENCES

[1] P. Mecenas, R. T. R. M. Bastos, A. C. R. Vallinoto, and D. Normando, "Effects of temperature and humidity on the spread of COVID-19: A systematic review," *PLoS One*, vol. 15, no. 9, 2020, Art. no. e0238339.
[2] C. Massaroni, M. Caponero, R. D. Amato, D. L. Presti, and E. Schena, "Fiber Bragg grating measuring system for simultaneous monitoring of temperature and humidity in mechanical ventilation," *Sensors*, vol. 17, no. 4, 2017, Art. no. 749.
[3] Y. Zhong, Z. Tong, W. Zhang, J. Qin, and W. Gao, "Humidity and temperature sensor based on a Mach-Zehnder interferometer with a pokal taper and peanut taper," *Appl. Opt.*, vol. 58, no. 29, pp. 7981–7886, 2019.
[4] Y. Wang, Y. Yan, Z. Lian, D. Chen, A. Pak Tao Lau, and C. Lu, "Fabry–Perot interferometers for highly-sensitive multi-point relative humidity sensing based on the vernier effect and digital signal processing," *Opt. Exp.*, vol. 30, no. 22, pp. 39946–39960, 2022.
[5] M. Lepore and I. Delfino, "Optical sensors technology and applications," *Sensors*, vol. 22, 2022, Art. no. 7905.
[6] R. Tong, Y. Zhao, H. Zheng, and F. Xia, "Simultaneous measurement of temperature and relative humidity by compact Mach-Zehnder interferometer and Fabry-Perot interferometer," *Measurement*, vol. 155, 2020, Art. no. 107499.
[7] R. Tong, Y. Zhao, M. Chen, X. Hua, and Y. Yang, "Simultaneous measurement of RH and temperature based on FBG and balloon-like sensing structure with inner embedded up-tapered MZI," *Measurement*, vol. 146, 2019, pp. 1–8.
[8] X. Ding, J. Yan, N. Chen, T. Jin, and R. Zhang, "Highly sensitive balloon-like fiber interferometer based on GO nanomaterial coated for humidity measurement," *Opt. Laser Technol.*, vol. 158, 2023, Art. no. 108798.
[9] Y. Wang, Q. Huang, W. Zhu, and M. Yang, "Simultaneous measurement of temperature and relative humidity based on FBG and FP interferometer," *IEEE Photon. Technol. Lett.*, vol. 30, no. 9, pp. 833–836, May 2018.
[10] H. Chen, C. Jiang, X. Zhu, X. Guo, H. Li, and S. Sun, "A parallel optical fiber fabry–perot interferometer for simultaneous measurement of relative humidity and temperature," *IEEE Sensors J.*, vol. 22, no. 18, pp. 17845–17853, Sep. 2022.

[11] F. Li et al., "Simultaneous measurement of temperature and relative humidity using cascaded C-shaped Fabry-Perot interferometers," *J. Lightw. Technol.*, vol. 40, no. 4, pp. 1209–1215, Feb. 2022.

[12] Y. Zhao, M. S. A. Gandhi, Q. LI, Z. LIU, and H. Y. Fu, "Vernier effect assisted sucrose sensor based on a cascaded Sagnac interferometer with no-core fiber," *Biomed. Opt. Exp.*, vol. 12, no. 12, pp. 7338–7347, 2021.

[13] Q. Liu et al., "Cascaded Sagnac loops embedded with two polarization maintaining photonic crystal fibers for highly sensitive strain measurement," *IEEE Trans. Instrum. Meas.*, vol. 70, 2021, Art. no. 7002309.

[14] L. Sun, J. Li, L. Jin, Y. Ran, and B. Guan, "High-birefringence microfiber Sagnac interferometer-based humidity sensor," *Sensors Actuators B*, vol. 231, pp. 696–700, 2016.

[15] S. Zhang, Y. Liu, H. Guo, A. Zhou, and L. Yuan, "Highly sensitive vector curvature sensor based on two juxtaposed fiber Michelson interferometers with vernier-like effect," *IEEE Sensors J.*, vol. 19, no. 6, pp. 2148–2154, Mar. 2019.

[16] Z. Li, Y. Zhang, W. Zhang, L. Kong, Y. Yue, and T. Yan, "Parallelized fiber Michelson interferometers with advanced curvature sensitivity plus abated temperature crosstalk," *Opt. Lett.*, vol. 45, pp. 4996–4999, 2020.

[17] X. Jia, X. Zhou, M. Bi, G. Yang, M. Hu, and T. Wang, "High-sensitivity optical fiber temperature sensor of cascaded FSI and MZI based on vernier effect," *Opt. Fiber Technol.*, vol. 65, 2021, Art. no. 102625.

[18] X. Zhou, Y. Zhou, Z. Li, M. Bi, G. Yang, and T. Wang, "Research on temperature sensing characteristics with cascaded fiber Sagnac interferometer and fiber Fabry-Perot interferometer-based fiber laser," *Opt. Eng.*, vol. 58, no. 5, Art. no. 102625.

[19] X. Jia, X. Zhou, J. Chen, M. Hu, and T. Wang, "Optical fiber temperature sensor based on vernier-effect FPI and MZI," *J. Optoelectron. Laser*, vol. 33, no. 1, pp. 9–13, 2022.

[20] A. D. Gomes et al., "Optical harmonic vernier effect: A new tool for high-performance interferometric fiber sensors," *Sensors*, vol. 19, 2019, Art. no. 5431.

[21] Y. Wang, X. Zhu, H. Chen, C. Jiang, X. Guo, and S. Sun, "Relative humidity sensor based on cascaded Fabry-Perot interferometers and vernier effect," *Optik*, vol. 254, 2022, Art. no. 168605.